Crystal structure of human ISG20, an interferon-induced antiviral ribonuclease

Tatsuya Horio*, Masatoshi Murai, Toshihiko Inoue, Tomohiro Hamasaki, Teruo Tanaka, Tadaaki Ohgi

Research Laboratories, Nippon Shinyaku Co. Ltd, 3-14-1 Sakura, Tsukuba, Ibaraki 305-0003, Japan

Received 29 July 2004; revised 10 September 2004; accepted 27 September 2004

Available online 12 October 2004

Edited by Irmgard Sinning

Abstract ISG20 is an interferon-induced antiviral exoribonuclease that acts on single-stranded RNA and also has minor activity towards single-stranded DNA. It belongs to the DEDDh group of RNases of the DEDD exonuclease superfamily. We have solved the crystal structure of human ISG20 complexed with two Mn^{2+} ions and uridine 5′-monophosphate (UMP) at 1.9 Å resolution. Its structure, including that of the active site, is very similar to those of the corresponding domains of two DEDDh-group DNases, the ε subunit of *Escherichia coli* DNA polymerase III and *E. coli* exonuclease I, strongly suggesting that its catalytic mechanism is identical to that of the two DNases. However, ISG20 also has distinctive residues, Met14 and Arg53, to accommodate hydrogen bonds with the 2′-OH group of the UMP ribose, and these residues may be responsible for the preference of ISG20 for RNA substrates.

Keywords: Crystal structure; Exonuclease; Interferon; ISG20

1. Introduction

Interferons comprise a family of secretory proteins characterized chiefly by their ability to induce cellular antiviral proteins. Among the well-studied interferon-induced antiviral proteins are the double-stranded RNA-dependent protein kinase PKR, the 2′,5′-oligoadenylate synthetase/RNase L system, and the Mx family of GTPases [1–4].

ISG20 (interferon-stimulated gene product of 20 kDa) is a protein induced by interferons or double-stranded RNA [5,6]. Its involvement in antiviral mechanisms was elucidated in a recent study [7], where it was demonstrated that overexpression of recombinant ISG20 in cultured cells increases cellular resistance to infection by some RNA genomic viruses. Moreover, mouse embryonic fibroblasts triply deficient in PKR, RNase L and Mx gene expression still exhibit residual antiviral activity, the extent of which is correlated with the amount of interferon-induced expression of endogenous ISG20 protein [7]. These facts suggest that ISG20 may participate in an alternative interferon-mediated antiviral pathway.

* Corresponding author. Fax: +81-29-850-6217.
E-mail address: t.horio@nippon-shinyaku.co.jp (T. Horio).

Abbreviations: UMP, uridine 5′-monophosphate

ISG20 is a 3′ to 5′ exonuclease with a strong preference for single-stranded RNA substrates and minor activity towards single-stranded DNA [8]. According to sequence-alignment analyses, ISG20 belongs to the DEDD superfamily, a 3′ to 5′ exonuclease superfamily defined by four conserved acidic residues, three aspartates (D) and one glutamate (E), distributed among three separate sequence motifs (ExoI–III) [9,10]. Exonucleases in this superfamily require two divalent metal ions for catalytic activity, and the four conserved residues play a crucial role in binding the metal ions at the active site. The DEDD superfamily can be subdivided into two groups, DEDDy and DEDDh, which are distinguished according to whether a fifth conserved residue is tyrosine (y) or histidine (h). These Tyr and His residues are also located at the active site and are presumed to play an equivalent role in activating the water molecule which is destined to attack the phosphorus atom in the target phosphodiester bond. While the DEDD superfamily includes both DNases and RNases, their substrate specificity is not correlated with their assignment to the DEDDy or the DEDDh group. For example, ISG20 and some other RNases such as RNase T and oligoribonuclease are included in the DEDDh group along with some DNases such as the proofreading domain of bacterial DNA polymerase III, while RNase D and the proofreading domains of A or B type DNA polymerases are included in the DEDDy group. Most current knowledge of the structure and catalytic mechanism of DEDD exonucleases is derived from studies of DNases [12–22] (Table 1); RNases in this superfamily have been far less well studied from a structural point of view, although the crystal structure of the RNase domain of *Saccharomyces cerevisiae* Pop2, a DEDD-superfamily-related protein with non-canonical active-site residues, has recently been reported [11].

We here report the crystal structure of human ISG20, a DEDDh-group RNase, complexed with two manganese ions and uridine 5′-monophosphate (UMP), a product of the exonuclease reaction, at 1.9 Å resolution. The structure of ISG20, especially around the active site, is similar to those of the corresponding domains of two DEDDh-group DNases (members of the DnaQ superfamily), the ε subunit of *Escherichia coli* DNA polymerase III [12] and *E. coli* exonuclease I [13], strongly suggesting that these three enzymes have a common catalytic mechanism. However, ISG20 recognizes the sugar moiety of the nucleotide in a slightly different manner from the two DNases, to accommodate hydrogen bonds with the ribose 2′-OH group of UMP. This

0014-5793/$22.00
doi:10.1016/j.febslet.2004.09.074

Table 1
Crystal-structural studies of DEDDh-group DNases

	Resolution (Å)	Ligand(s)	PDB code	Reference
E. coli DNA polymerase III ε subunit N-terminal domain (ε186)	1.8/1.7[a] (pH 8.5/pH 5.8)	Two Mn^{2+} ions and dTMP	1J53/1J54[a]	[12]
E. coli exonuclease I (ExoI)	2.4	One Mg^{2+} ion	1FXX	[13]

[a] The structure was solved at different pH values.

mode of binding can explain the preference of ISG20 for RNA substrates.

2. Materials and methods

2.1. Purification and crystallization

The gene coding for human ISG20 was cloned into the expression vector pET28a (Novagen, Madison, WI, USA) as described elsewhere [8]. The ISG20 protein, tagged with six histidine residues at the C-terminus, was expressed in the *E. coli* strain BL21 (DE3) (Novagen) and purified on a nickel-chelating affinity column (His·Bind Fractogel; Novagen) and a cation-exchange column (HiTrap SP HP; Amersham Biosciences, Piscataway, NJ, USA). The purified protein was concentrated to 15 mg/ml in 0.1 M sodium acetate, pH 5.5, containing 0.3 M NaCl with Centriprep and Centricon centrifugal filter units (Millipore, Billerica, MA, USA). Protein solution (0.5 μl) was mixed with an equal volume of crystallization solution (0.2 M sodium acetate, pH 5.5, containing 2.6–2.9 M NaCl and 0.8% (v/v) 1-butanol) and equilibrated against the crystallization solution for about 1 h by the hanging drop vapor diffusion method, after which crystallization was initiated by microseeding. After 3–4 days at 23 °C, hexagonal needle-shaped crystals 0.5–1.0 mm in length and 0.05 mm in width were obtained.

2.2. Diffraction measurement and data processing

All diffraction data were collected at the BL32B2 beamline of the SPring-8 synchrotron radiation facility (Hyogo, Japan) with a Rigaku R-AXIS V imaging plate detector. For data collection at 100 K, a crystal was transferred to cryoprotectant (crystallization solution containing 30% glycerol) and, after twenty to thirty seconds, flash-cooled in a liquid-nitrogen gas stream. Diffraction data were processed with the HKL2000 package [23]. The ISG20 crystal had unit-cell dimensions of $a = b = 63.1$ Å and $c = 97.8$ Å in space group $P3_221$, with one molecule per asymmetric unit. The calculated solvent content of the crystal was 53%.

2.3. MAD data collection and MAD phasing

To determine the structure by the multiple-wavelength anomalous-dispersion (MAD) method, the Hg derivative was prepared by soaking a crystal in crystallization solution containing 10 mM mercury (II) acetate for about 35 h. From this crystal, the same 60° wedge of data was collected at each of the three wavelengths (edge = 1.0085 Å, peak = 1.0050 Å, and remote = 0.92 Å) (Table 2). Heavy-atom search and phase calculations were carried out with the CNX package (Accelrys Inc., San Diego, CA, USA). From the correspondence of the significant peaks of the dispersive and anomalous difference Patterson maps, it could be determined that there was one Hg atom site per ISG20 molecule. MAD phases were calculated to 2.5 Å resolution and improved by solvent flipping, yielding an electron-density map of good quality. On the basis of this map, an initial model was built with the program Turbo-Frodo [24].

2.4. Refinement of the structure as an ISG20–Mn^{2+}–UMP complex

To refine the crystal structure as a complex with Mn^{2+} ions and uridine 5′-monophosphate (UMP), the data were collected at a wavelength of 1.0 Å, with a crystal which had been soaked for 2.5 h in crystallization solution supplemented with 10 mM $MnCl_2$ and 10 mM UMP (Table 2). Five percent of the data was set aside for the calculation of R_{free} and the remainder used to refine the initial model at a resolution of 1.9 Å with the programs CNX and Turbo-Frodo. An initial round of rigid-body refinement was followed by repeated cycles of simulated annealing, B-factor refinement and model rebuilding, with the last cycle including water-picking. The final model contains residues 6–122 and 128–178 out of a total of 181 residues in the original human protein and has two Mn^{2+} ions and one UMP molecule at its active site (Fig. 1). Residues 123–127 were disordered and were therefore excluded from the model. Sufficient electron density was also not observed for the side chains of Glu6, Glu22, Gln62 and Arg171, so these residues were built as Ala residues. Ramachandran plots were analyzed by the program PROCHECK [25]. The refinement statistics are summarized in Table 3.

2.5. Identification of manganese ions

To locate the Mn^{2+} ions in the crystal structure of the ISG20–Mn^{2+}–UMP complex, the data were collected at a wavelength of 1.7 Å, near the K-absorption edge of Mn [26], from an ISG20–Mn^{2+}–UMP complex crystal prepared as described above. The anomalous difference Fourier map showed two large peaks in the region corresponding to the active site (Fig. 1). In order to identify Mn^{2+} ions unambiguously, data collection at wavelengths on both sides of the K-absorption edge of Mn is usually necessary. However, the heights of these two peaks were much greater than those of the peaks of the sulfur atoms of the Met and Cys residues, and therefore two Mn^{2+} ions can reasonably be assigned to these positions [27]. In addition to these two Mn^{2+} ions, another Mn^{2+} ion associated with a slightly smaller, diffuse peak was

Table 2
Data collection and MAD phasing statistics

	Hg(II) acetate			Native (complex)	Native (complex) (identification of Mn^{2+})
	Edge	Peak	Remote		
Wavelength (Å)	1.0085	1.0050	0.92	1.0	1.7
Cell dimensions *a*, *c* (Å)	63.1, 97.8	63.1, 97.8	63.1, 97.8	63.42, 97.91	63.3, 97.8
Resolution range (Å)	50–2.5 (2.59–2.5)	50–2.5 (2.59–2.5)	50–2.5 (2.59–2.5)	50–1.9 (1.97–1.9)	50–2.5 (2.59–2.5)
No. of observed reflections	28 074	28 167	28 163	65 192	25 869
No. of unique reflections	8188	8175	8197	18 442	7900
Completeness (%)	99.9 (99.9)	99.9 (100)	99.9 (100)	99.6 (100)	95.7 (94.1)
$I/\sigma(I)$	13.5 (8.4)	13.5 (8.4)	13.6 (8.5)	23.9 (9.8)	19.1 (7.5)
R_{sym} (%)[a]	6.2 (12.1)	6.6 (12.8)	6.1 (12.2)	3.9 (17.4)	5.3 (19.6)
Phasing power, iso/ano	0.98/2.13	0.72/2.14	–/1.89		
Figure of merit	–	–	0.60		

Values in parentheses refer to the highest-resolution shell.
[a] $R_{sym} = (\sum |I - \langle I \rangle|)/(\sum I)$, where I is the observed intensity and $\langle I \rangle$ is the average intensity of symmetry-related reflections.

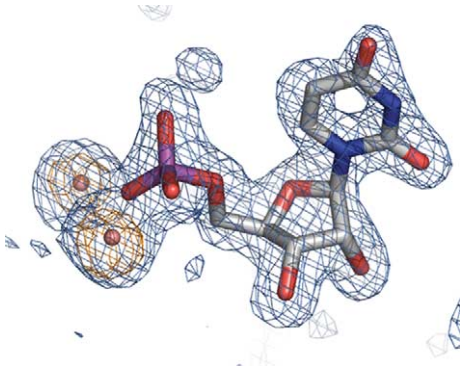

Fig. 1. A simulated annealing $F_o - F_c$ omit electron-density map of the region of the active site contoured at 2 σ (blue), generated by omitting UMP and the two Mn^{2+} ions from the phase calculation. Superimposed on this is an anomalous difference Fourier electron density map of the same region contoured at 10 σ (orange), calculated from the data collected at a wavelength of 1.7 Å. UMP in the final model is shown in stick representation and the two Mn^{2+} ions as small spheres. Figs. 1–5 were generated with the PyMOL Molecular Graphics System (DeLano Scientific, San Carlos, CA, USA; http://www.pymol.org) and the ray-tracing renderer POV-ray (http://www.povray.org).

found between the side chains of Asp90 and His93 (not shown). Although this Mn^{2+} ion was probably not specifically bound to these side chains, it was included in the refinement. The atomic coordinates of the structure have been deposited in the Protein Data Bank (PDB) with the accession code 1WLJ.

3. Results and discussion

3.1. Overall structure

The crystal structure of the ISG20–Mn^{2+}–UMP complex determined by the MAD method at 1.9 Å resolution (Fig. 2A) can be seen to consist of a core five-stranded β-sheet with one antiparallel strand (β2) and seven α-helices, with groups of two (α3, α4) and five (α1, α2, α5–α7) helices on opposite sides of the surface of the sheet. The whole molecule has a somewhat elongated, flat shape with approximate dimensions of $50 \times 32 \times 21$ Å^3. The active site is located in the hollow near

Table 3
Refinement statistics

Resolution range (Å)	20–1.9
No. of reflections, working set/test set	17 487/937
R_{work}/R_{free}	0.207/0.227
No. of refined atoms	
Protein atoms	1313
Solvent atoms	83
Mn and UMP atoms	24
Average *B*-factor (Å^2)	21.2
Rms deviations from ideality	
Bond lengths (Å)	0.006
Bond angles (°)	1.2
Dihedral angles (°)	22.6
Improper angles (°)	0.73
Ramachandran plot (%)	
Most favored region	91.2
Additional allowed region	8.8

center of the molecule surrounded by β1, α1, α4, and the N-terminal region of α7. When this structure is compared with the crystal structures of two DNases in the DEDDh group, the catalytic N-terminal domain of the ε subunit of *E. coli* DNA polymerase III (called ε186; Fig. 2B) [12] and the *E. coli* exonuclease I (abbreviated ExoI) exonuclease domain (Fig. 2C) [13], the spatial arrangement of their secondary-structure elements can be seen to be very similar in spite of the low sequence identity (~15%) and similarity (~35%) between ISG20 and these DNase domains. Of the 168 Cα atoms in our ISG20 model, 138 can be superimposed on the corresponding Cα atoms of ε186 with a root-mean-square deviation (r.m.s.d.) of 2.15 Å, while 132 can be superimposed on the corresponding Cα atoms of ExoI with a r.m.s.d. of 2.25 Å (Fig. 3).

However, there are several differences between ISG20 and the two DNases (Fig. 2). First, the loop segment connecting β4 and β5 in ISG20 is rather short, so that, compared to the two DNases, ISG20 has a short α4 helix and lacks the 3_{10} helix that the DNases have in this segment. Second, β1–β3 in ISG20 form a longer and more twisted β-sheet than they do in the two DNases, and this also generates differences in the structures of the loop segments connecting these β-strands. In addition, the

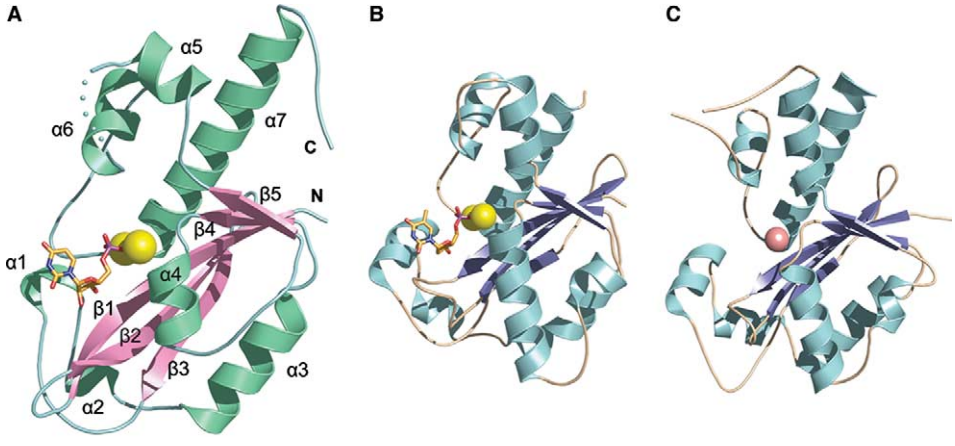

Fig. 2. Ribbon diagrams based on the crystal structures of (A) human ISG20, (B) the N-terminal domain of the *E. coli* DNA polymerase III ε subunit (ε186; PDB code 1J54 [12]), and (C) the N-terminal exonuclease domain of *E. coli* ExoI (PDB code 1FXX [13]). In (A) and (B), nucleotides and Mn^{2+} ions bound at the active sites are shown in stick and sphere representations, respectively. The sphere in (C) represents a Mg^{2+} ion found in the active site of ExoI.

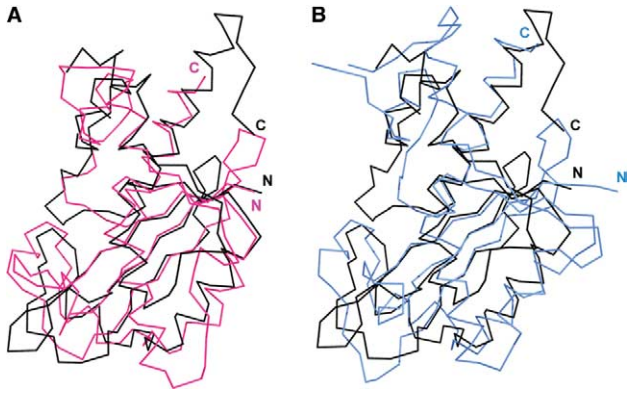

Fig. 3. Superposition of the Cα traces of (A) ISG20 (black) and ε186 (pink), and (B) ISG20 (black) and the exonuclease domain of ExoI (blue).

α5 helix of ISG20 extends in a slightly different direction from the α5 helix of the two DNases.

3.2. Structure of the active site

Previous structural studies on the Klenow fragment of *E. coli* DNA polymerase I, whose proofreading domain belongs to DEDDy-group DNases, have shown that dTMP, a product of the exonuclease reaction, binds at nearly the same position as the 3′-terminal nucleotide of the DNA substrate [14–16]; and this compound has also been used for the structural study of ε186 [12]. We used UMP instead of dTMP, because ISG20 is known to show a marked preference for RNA substrates. In addition to UMP, manganese ions, which are essential for the catalytic activity of ISG20 [8], were added to the soaking solution to prepare an ISG20–Mn^{2+}–UMP-complex crystal. According to the structure we have determined for the ISG20–Mn^{2+}–UMP complex, the two Mn^{2+} ions, Mn A and Mn B, lie about 3.8 Å apart in the active site (Fig. 4A). DEDDh exonucleases have five invariant residues that are crucial for the structure of the active site [9]. Corresponding to these residues in ISG20 are Asp11, Glu13, Asp94, His149 and Asp154. Our model shows that the ligands to Mn A are carboxylate oxygens of Asp11, Glu13 and Asp154 and oxygens O2P and O3P of the UMP phosphate group. The ligands to Mn B are the other carboxylate oxygens of Asp11, O3P of the UMP phosphate group, and four water oxygens, with these ligands having an octahedral coordination geometry. Of the four water molecules coordinated to Mn B, two are held by hydrogen bonds with carboxylate oxygens of Asp94. Comparison of this active site structure with that of ε186 clearly shows that the arrangement of the five invariant residues is very similar (Fig. 4), and comparison with ExoI (not shown) also reveals a similar arrangement of these invariant residues. The crystal structure of ε186 has been solved at two different pH values, 5.8 and 8.5 [12] (Table 1), and the structure shown in Fig. 4B is the one solved at pH 5.8. The structures of ε186 at the two different pH values are nearly identical, but there is a small difference in the mode of binding of the phosphate group of dTMP at the active site [12,17]. In our ISG20 model, the manner in which UMP interacts with Mn^{2+} ions and the five invariant residues at pH 5.5 is almost identical to the manner in which dTMP interacts with ε186 at pH 5.8. The high similarity of the active-site structures of ISG20 and ε186 strongly suggests that the five invariant residues in these enzymes fulfill the same catalytic roles in the respective exonuclease reactions, and therefore that the catalytic mechanisms are probably identical.

It is worth noting that His149 Nδ of ISG20 forms a hydrogen bond with O2P of the UMP phosphate group. The equivalent hydrogen bond is also observed in ε186 at pH 5.8, and it is considered to be one piece of evidence for the importance of this histidine residue in the catalytic mechanism [12]. According to the mechanism proposed for ε186, a water molecule (or hydroxide ion) is activated by His162 Nδ and Mn A, and carries out a nucleophilic attack on the phosphorus atom of the 3′-terminal phosphodiester group; the water molecule thereby contributes a 5′-monophosphate oxygen to the mononucleotide product, corresponding to O2P of dTMP (Fig. 4B) [12,17]. This mechanism is the same for DNA and RNA substrates, so that the residues involved in distinguishing these substrates must be present in an area other than the active center.

3.3. Interaction with the nucleotide sugar moiety

ISG20 and ε186 interact with the sugar moiety of the nucleotide product as well as with the phosphate moiety. In ISG20, Glu13 Oε1 and the main-chain nitrogen of Met14 are

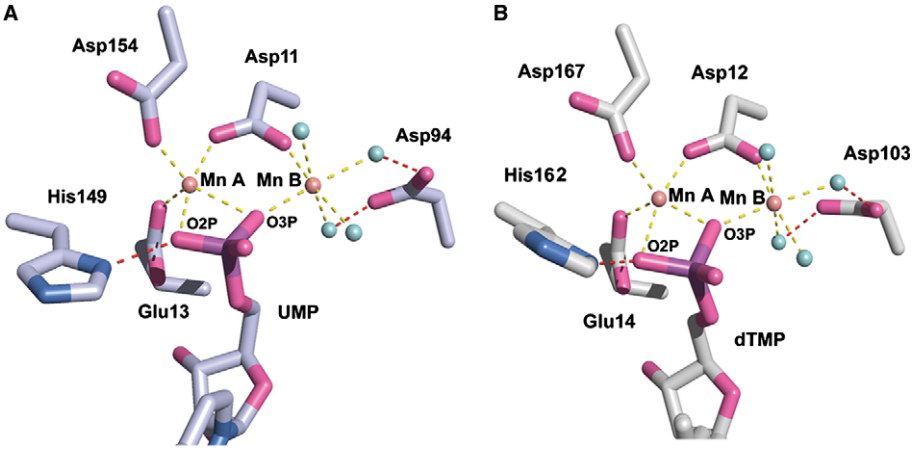

Fig. 4. Active-site structures of (A) ISG20 and (B) ε186. Small blue spheres represent water molecules. Coordinate bonds between Mn^{2+} ions and ligands are shown as yellow dotted lines and hydrogen bonds as red dotted lines.

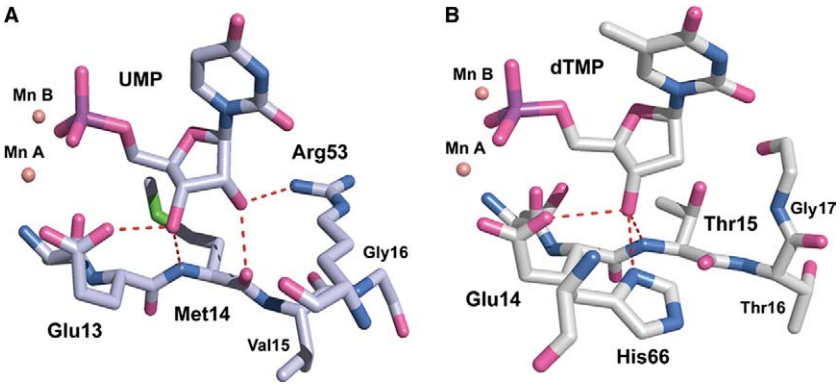

Fig. 5. Interactions between (A) UMP ribose and ISG20 and (B) dTMP deoxyribose and ε186. Hydrogen bonds are shown as red dotted lines.

within hydrogen-bonding distance of the ribose 3′-OH (2.5 and 2.8 Å, respectively), whereas the main-chain carbonyl oxygen of Met14 and Nη1 of Arg53 are within hydrogen-bonding distance of the ribose 2′-OH (2.6 and 2.8 Å, respectively) (Fig. 5A). In ε186, the deoxyribose 3′-OH of dTMP is observed to make three hydrogen bonds, one with Glu14 Oε1, one with the main-chain nitrogen of Thr15, and one with His66 Nδ (Fig. 5B) [12]. Given that Glu13 and Met14 of ISG20 correspond to Glu14 and Thr15 of ε186, the two enzymes interact with the sugar 3′-OH group in a parallel manner, except for the extra hydrogen bond with His66 in ε186. The fact that ISG20 can form two extra hydrogen bonds with the 3′-terminal nucleotide of RNA substrates leads one to expect that RNA would be accommodated more favorably than DNA, consistent with the observation that ISG20 degrades RNA far more rapidly than DNA [8]. In ε186, in contrast, RNA substrates are not likely to be accommodated stably in the crystal structure, because of the expected steric repulsion between the ribose 2′-OH and Thr15 Oγ. Instead, the side chain of His66, which has no counterpart in ISG20, reinforces the interaction of ε186 with DNA substrates. On these grounds, DNA would be expected to be a more suitable substrate for ε186, in accordance with the known activity of this exonuclease.

The side chain of Arg53 intrudes into the active site and makes a hydrogen bond with the ribose 2′-OH. In ε186 and ExoI, the position equivalent to the side chain of Arg53 is occupied by a part of the protruding loop segment between β1 and β2. However, in ISG20 the corresponding segment forms an extended β-sheet and cannot protrude into that position. An assessment of whether the equivalent Arg residue is present in the other DEDD RNases based solely on sequence alignment is difficult because of the low sequence identity between ISG20 and the other DEDD RNases, but *S. cerevisiae* Rex4, a DEDDh RNase with ~40% sequence identity to ISG20 [28], is predicted to have the equivalent Arg residue. Meanwhile, an equivalent residue is not found in the active site in the crystal structure of Pop2, a DEDD-superfamily-related RNase [11].

Met14 is another notable residue, and its side chain occupies a position that allows a hydrogen bond between the ribose 2′-OH and the main-chain oxygen of this residue, in contrast to the corresponding side chain of Thr15 in ε186, which would clash with the ribose 2′-OH of RNA substrates. Met14 of ISG20 and Thr15 of ε186 are the residues immediately following the invariant Glu residue that is found in the active site. The position of this Glu residue in the active site is considered to be highly conserved in the DEDD exonucleases, so the residue that directly follows this Glu residue in the sequence is also expected to occupy a conserved position. Inspection of the sequence of DEDD exonucleases shows that DNases tend to have a Thr residue just after the invariant Glu residue, whereas RNases tend to have a residue other than Thr. The only apparent exception is the members of the RNase T subfamily, which do have a Thr residue at this position. However, it is reported that RNase T actually has higher activity towards DNA substrates than RNA substrates [29]. All these facts suggest that the presence of a Thr residue at this position in DEDD exonucleases is unfavorable to the binding of RNA substrates. Further study to investigate the putative role of Arg53 and Met14 of ISG20 in the recognition of RNA substrates would be of interest. In particular, mutating Arg53 to another residue, and perhaps also mutating Met14 to a Thr residue, may be expected to substantially reduce the activity of ISG20 towards RNA substrates.

ISG20 has no residue to interact with the uracil part of UMP, and residues that would be predicted to interact with other bases are also not found. This result is consistent with the fact that ISG20 is not a sequence-specific nuclease [8].

ISG20 is assumed to degrade viral or cellular RNA and to contribute to the suppression of viral replication. The results of our structural study suggest a rational explanation for ISG20's intrinsic preference for RNA substrates and its sequence-independent activity, properties expected to be critical for its physiological role as an antiviral protein.

Acknowledgements: We thank the staff of the BL32B2 beamline at the SPring-8 facility for their help in collecting the data. We also thank Dr. G.E. Smyth (Research Laboratories, Nippon Shinyaku) for critical reading of the manuscript.

References

[1] Samuel, C.E. (2001) Clin. Microbiol. Rev. 14, 778–809.
[2] Clemens, M.J. (1997) Int. J. Biochem. Cell Biol. 29, 945–949.
[3] Player, M.R. and Torrence, P.F. (1998) Pharmacol. Ther. 78, 55–113.
[4] Haller, O. and Kochs, G. (2002) Traffic 3, 710–717.
[5] Gongora, C., David, G., Pintard, L., Tissot, C., Hua, T.D., Dejean, A. and Mechti, N. (1997) J. Biol. Chem. 272, 19457–19463.
[6] Espert, L., Rey, C., Gonzalez, L., Degols, G., Chelbi-Alix, M.K., Mechti, N. and Gongora, C. (2004) Oncogene 23, 4636–4640.

[7] Espert, L., Degols, G., Gongora, C., Blondel, D., Williams, B.R., Silverman, R.H. and Mechti, N. (2003) J. Biol. Chem. 278, 16151–16158.
[8] Nguyen, L.H., Espert, L., Mechti, N. and Wilson, D.M., III (2001) Biochemistry 40, 7174–7179.
[9] Zuo, Y. and Deutscher, M.P. (2001) Nucleic Acids Res. 29, 1017–1026.
[10] Moser, M.J., Holley, W.R., Chatterjee, A. and Mian, I.S. (1997) Nucleic Acids Res. 25, 5110–5118.
[11] Thore, S., Mauxion, F., Seraphin, B. and Suck, D. (2003) EMBO Rep. 4, 1150–1155.
[12] Hamdan, S., Carr, P.D., Brown, S.E., Ollis, D.L. and Dixon, N.E. (2002) Structure 10, 535–546.
[13] Breyer, W.A. and Matthews, B.W. (2000) Nat. Struct. Biol. 7, 1125–1128.
[14] Derbyshire, V., Freemont, P.S., Sanderson, M.R., Beese, L., Friedman, J.M., Joyce, C.M. and Steitz, T.A. (1988) Science 240, 199–201.
[15] Beese, L.S. and Steitz, T.A. (1991) EMBO J. 10, 25–33.
[16] Brautigam, C.A. and Steitz, T.A. (1998) J. Mol. Biol. 277, 363–377.
[17] Hamdan, S., Bulloch, E.M., Thompson, P.R., Beck, J.L., Yang, J.Y., Crowther, J.A., Lilley, P.E., Carr, P.D., Ollis, D.L., Brown, S.E. and Dixon, N.E. (2002) Biochemistry 41, 5266–5275.
[18] Wang, J., Yu, P., Lin, T.C., Konigsberg, W.H. and Steitz, T.A. (1996) Biochemistry 35, 8110–8119.
[19] Kiefer, J.R., Mao, C., Hansen, C.J., Basehore, S.L., Hogrefe, H.H., Braman, J.C. and Beese, L.S. (1997) Structure 5, 95–108.
[20] Freemont, P.S., Friedman, J.M., Beese, L.S., Sanderson, M.R. and Steitz, T.A. (1998) Proc. Natl. Acad. Sci. USA 85, 8924–8928.
[21] Brautigam, C.A., Sun, S., Piccirilli, J.A. and Steitz, T.A. (1999) Biochemistry 38, 696–704.
[22] DeRose, E.F., Li, D., Darden, T., Harvey, S., Perrino, F.W., Schaaper, R.M. and London, R.E. (2002) Biochemistry 41, 94–110.
[23] Otwinowski, Z. and Minor, W. (1997) Methods Enzymol. 276, 307–326.
[24] Roussel, A. and Cambillau, C. (1989) Silicon Graphics Geometry Partner Directory, pp. 77–78, Silicon Graphics, Mountain View, CA.
[25] Laskowski, R.A., McArthur, M.W., Moss, D.S. and Thornton, J.M. (1993) J. Appl. Crystallogr. 26, 283–291.
[26] Einspahr, H., Suguna, K., Suddath, F.L., Ellis, G., Helliwell, J.R. and Papiz, M.Z. (1985) Acta Crystallogr. B 41, 336–341.
[27] Weiss, M.S., Panjikar, S., Nowak, E. and Tucker, P.A. (2002) Acta Crystallogr. D 58, 1407–1412.
[28] Eppens, N.A., Faber, A.W., Rondaij, M., Jahangir, R.S., van Hemert, S., Vos, J.C., Venema, J. and Raue, H.A. (2002) Nucleic Acids Res. 30, 4222–4231.
[29] Zuo, Y. and Deutscher, M.P. (1999) Nucleic Acids Res. 27, 4077–4082.